High-energy, mid-IR, picosecond fiber-feedback optical parametric oscillator

YUDI WU, SIJING LIANG, QIANG FU, THOMAS D. BRADLEY, FRANCESCO POLETTI, DAVID J. RICHARDSON AND LIN XU*

Optoelectronics Research Centre, University of Southampton, Southampton, SO17 1BJ, UK
**Corresponding author: L.Xu@soton.ac.uk*

Received XX Month XXXX; revised XX Month, XXXX; accepted XX Month XXXX; posted XX Month XXXX (Doc. ID XXXXX); published XX Month XXXX

A compact, mid-infrared (MIR), synchronously pumped, fiber-feedback optical parametric oscillator (OPO) based on periodically poled lithium niobate is developed with tunable signal and idler wavelength ranges of 1472.0 - 1758.2 nm and 2559.1 - 3562.7 nm, respectively. A solid-core SMF-28 fiber and a hollow-core fiber were used as the feedback-fibers in order to compare the effect of their substantially different levels of nonlinearity. The OPO generates 1-MHz, 120-ps, MIR pulses with up to 1.50-μJ pulse energy and 11.7-kW peak power.

http://dx.doi.org/10.1364/OL.99.099999

Short-pulsed MIR lasers have many important applications in the areas such as spectroscopy, material processing, free-space communications and medical treatment [1-4]. Synchronously pumped optical parametric oscillators (SPOPOs) are commonly used as short-pulsed MIR laser sources through frequency conversion of readily available near infrared lasers. However, SPOPOs require temporal synchronization between the pump and the resonated signal when used to produce ultrashort pulses. Hence, a long cavity length is required when pumped with high-energy pulses at low repetition rate. For example, a SPOPO operating at 100 MHz repetition rate requires a 3-m-long cavity [5], whereas a cavity length of 8.16 m is needed to achieve a repetition rate of 36.7 MHz [6]. It can be seen that with further reduction of repetition rate, conventional free-space SPOPOs would require a very long cavity that would normally impose great physical and practical issues.

We have previously demonstrated various techniques to increase the compactness of such OPOs operating at low repetition rate. For example, a high-harmonic cavity, in which the cavity length was set to be a fraction of the length required for synchronous pumping, was used to operate at repetition rate of 1 MHz [7], achieving MIR idler pulse energies up to 1.5 μJ and 9.4 kW corresponding peak power. However, using a high-harmonic cavity increased the pump threshold and also restricted the resonated signal output due to the requirement of a high reflectivity (HR) cavity for the signal. In another demonstration, a compact SPOPO with high-peak-power output was realized in burst-mode operation, in which the OPO was pumped by a burst of pulses with a high intra-burst pulse repetition rate but a low inter-burst pulse repetition rate [8]. Through this method, controllable MIR idler peak power of up to 8.4 kW (0.38 μJ pulse energy) was achieved. However, the cavity signal oscillation must be re-established at every burst, which caused a variation in pulse amplitude across each burst window.

An alternative method to reduce the footprint of SPOPOs is to use a piece of optical fiber inside the cavity to replace the free-space beam path for synchronous pumping [9, 10]. Apart from creating the temporal delay, silica fiber has large material group velocity dispersion and can be used to manage the intra-cavity dispersion within femtosecond OPOs [11, 12]. In the hundreds-of-picosecond regime, where dispersion is less critical, a fiber-feedback OPO has been demonstrated at a repetition rate of 7.19 MHz using a 42-m length of single-mode fiber and generated MIR idler pulses with a peak power of up to 1.8 kW (0.19 μJ pulse energy) [13]. However, nonlinear temporal and spectral distortions caused by propagation in the required long lengths of standard silica fiber, can limit the power-scaling in such laser systems.

Here, for the first time to the best of our knowledge, we report a compact fiber-feedback OPO, synchronously pumped at a 1-MHz repetition rate, achieving MIR pulse energies up to 1.5 μJ at 2950 nm. These results represent the highest energy MIR pulses achieved from such structured OPOs to date. To match the low repetition rate, a ~200-m long single-mode fiber (SMF) was initially used inside the OPO cavity, which resulted in significant spectral broadening due to the relatively high nonlinearity of the SMF and high intracavity powers. In comparison, a ~300-m-long hollow-core fiber (HCF) was employed thereby reducing the nonlinearity of the fiber delay line by several orders of magnitude, and allowing for the possibility of further power-scaling high-brightness fiber-feedback OPOs.

The OPO pump source is an in-house-built fully polarization maintaining (PM) ytterbium-doped-fiber (YDF) master-oscillator-power-amplifier (MOPA) system, seeded by a 1040-nm gain-

switched laser-diode (GSLD). A schematic of the MOPA system is illustrated in Fig. 1. The GSLD (1064CHP, 3SPhotonics) seed laser was operated at a 64.0-MHz repetition rate, producing 120-ps pulses at 1040 nm, with a 0.38-mW average output power. Aside from the GSLD, the MOPA comprised four YDF amplifier stages and an electro-optic modulator (EOM). The MOPA incorporates core-pumped PM YDFs (PM-YDF-5/130-VIII, Nufern) with a 5-μm core diameter in the first and the second amplifier stages, a cladding-pumped PM YDF (PMLA-YDF-10/125-VIII, Nufern) with an 11-μm core and 125-μm cladding diameter in the third stage, and a cladding-pumped PM YDF (PMLA-YDF-25/250-VIII, Nufern) with a 25-μm core and 250-μm cladding diameter in the fourth stage. The pump laser diodes (LDs) used in the MOPA amplification stages were 980-nm single-mode LDs with 200-mW launch power in the first and second stages, a 976-nm multi-mode LD with 1.5-W launch power in the third stage, and a 975-nm wavelength-stabilized multi-mode LD providing 20-W launch power in the fourth stage, respectively. The core-pumped YDFs used in the first and second-stage amplifiers had lengths of 80 cm, and the lengths of cladding pumped YDFs used in the third and fourth stage amplifiers were both 2.5 m. An electro-optic modulator (EOM) was inserted between the first and second amplification stages and was used as a pulse picker to reduce the pulse repetition rate down to 1 MHz. The MOPA provided an average output power of up to 7.3 W in a linearly polarized beam with a diffraction limited beam quality (M^2 ~ 1.02).

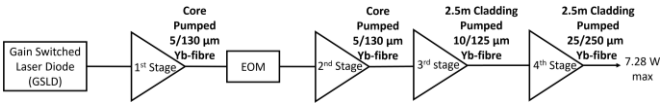

Fig. 1. Schematic of the fiber MOPA system.

Figure 2(a) shows the output spectrum at different powers from the MOPA. Self-phase-modulation (SPM) induced spectral broadening was observed due to the high peak powers (inset of Fig. 2(a)). At 7.3-W average power, the 10-dB spectral linewidth was 0.6 nm, and further increase of the output power would have resulted in a spectral linewidth beyond the estimated pump acceptance bandwidth of the nonlinear crystal used in the OPO. The MOPA output pulse was measured using a 32-GHz-bandwidth photo-detector (83440D, Agilent) and a 20-GHz-bandwidth digital communication analyzer (Infiniium 86100C, Agilent), showing a pulse duration of 120ps as seen in Fig. 2(b), which is similar to that of the GSLD seed. To control the polarization for pumping the OPO, a half-wave plate was placed at the MOPA output (HWP in Fig. 3).

The OPO was of a signal-resonant ring-cavity design, consisting of two concave mirrors, two plane mirrors, an optical fiber, and a periodically poled lithium niobate (PPLN) nonlinear crystal. A schematic of the OPO cavity is presented in Fig. 3. Both concave mirrors (CM1 and CM2 in Fig. 3) had a radius of curvature of 250 mm and were of HR (>99 %) at wavelengths around 1.5 μm (signal) and provided ~81 % transmission at wavelengths around both 1 μm (pump) and 3 μm (idler). The plane mirror (M3 in Fig. 3) was a silver mirror of high reflectivity (>99 %) at all the wavelengths involved (i.e. pump, signal and idler). An output coupler of 90% signal transmission (OC in Fig. 3) was used to allow signal light to be coupled out of the cavity and to reduce intracavity signal peak power. The total free-space length of the OPO cavity was 1.58 m.

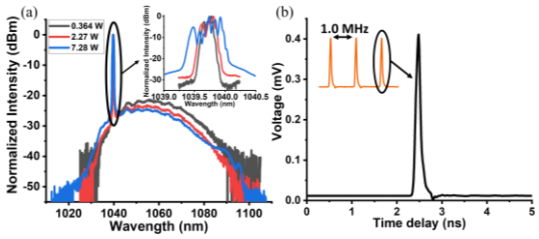

Fig. 2. Measured (a) Optical spectra of the MOPA output at different powers (inset shows the signal peak with a higher spectral resolution) and (b) optical pulse of the MOPA output (inset shows the 1-MHz pulse train).

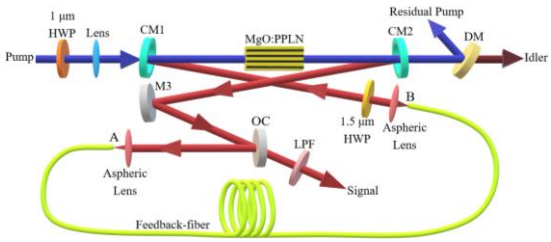

Fig. 3. Schematic of the OPO. HWP: Half-waveplate; CM1, CM2: concave mirrors; M3: plane mirror; OC: 90 % output coupler; DM: 45° Dichroic mirror; LPF: Long pass filter.

To match the pump to the signal cavity mode, which had a calculated beam radius of 116 μm at the centre of the PPLN crystal, the MOPA output beam was focused down to a measured beam radius of 117 μm with a plano-convex lens of 200-mm focal length. The 40-mm-long PPLN crystal (MOPO1-1.0-10, Covesion), had 5 poled gratings with periods ranging from 29.52 – 31.59 μm in steps of 0.5 μm. The crystal was mounted in an oven that allowed temperature tuning from 20 to 200 °C.

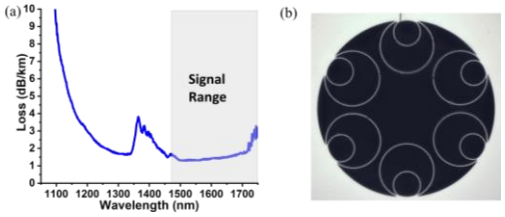

Fig. 4. (a)Cutback plot of the HCF fiber used in the fiber-feedback OPO cavity and (b) the HCF fiber cross-section.

Initially, a piece of standard telecommunications SMF (SMF-28) that had < 0.3 dB/km loss at 1500 nm – 1700 nm (signal) was used as the feedback fiber. Taking account of the silica refractive index, a fiber length of 203 m was selected to allow for synchronous pumping at 1 MHz. At points A and B of the OPO cavity (Fig. 3), aspheric lenses of 4.5-mm focal length were used to couple the signal in and out of the feedback fiber while matching the cavity mode. A 1.5 μm HWP was placed at the fiber output to control the polarization of the signal leaving the fiber. In later experiments the solid core SMF-28 feedback fiber was replaced by an in-house made HCF. The HCF used is a nested anti-resonant nodeless fiber (NANF) [14]. The cross-section of the NANF is presented in the inset of Fig.

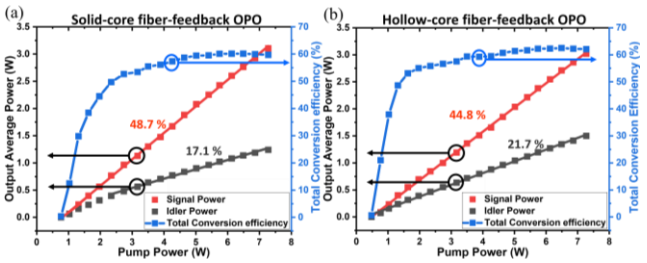

Fig. 5. Average idler power with linear fit (black), average signal power with linear fit (red) and conversion efficiency (blue dots) against pump power for a) the solid-core fiber-feedback OPO and b) the HCF fiber-feedback OPO. The blue line is a guide for the eye only.

4(b). The light was confined to the central void by the presence of the 6 non-contacting nested tube elements through coherent antiresonant reflection as determined by the thickness of the membrane elements [15]. The NANF fiber used here was of 33.5-μm core diameter and was single mode with < 2 dB/km loss at 1500 nm – 1700 nm (signal), as shown in the cutback plot in Fig. 4(a). This change was made to reduce the OPO's intracavity nonlinearities. A length of 298 m HCF was chosen for the OPO to match with the pump repetition rate when an effective refractive index being close to 1 was taken into account. Apart from 30-dB lower nonlinearity, the HCF had a group velocity dispersion (-3.5 fs^2/mm) about 6 times smaller than the SMF-28 (-23 fs^2/mm), which is highly beneficial in realizing such short-pulsed OPOs. Note that due to the larger core size of the HCF, the 4.5-mm focal length aspheric lenses were replaced by 9.8-mm aspheric lenses to match the signal cavity mode.

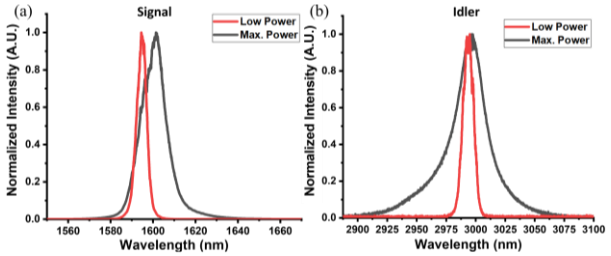

Fig. 6. Spectra of (a) signal and (b) idler for the solid-core fiber-feedback OPO at maximum and low powers.

For the idler measurements, a 45° dichroic mirror (DM in Fig. 3) of high reflectivity at 1 μm and 68.8 % transmission at 3 μm, was placed after the OPO cavity to filter out the residual pump light. A long-pass filter of high reflectivity at 1 μm and 86.1 % transmission at 1.5 μm, was placed after the output to allow signal measurements.

The OPO operation, using the SMF, was observed at a pump threshold of 0.77-W average power using a 30.49-μm PPLN grating at an oven temperature of 100 °C. The idler output power (black), taking into account the loss of CM2 and DM, and the signal output power (red) with respect to different pump powers is shown in Fig. 5(a). In theory the full idler power could be accessible if CM2 and DM had an idler transmission nearer to 100 %. The idler power increased linearly with respect to the pump power at a slope efficiency of 17.1 % up to a maximum power of 1.24 W, and the signal power also increased linearly with respect to the pump

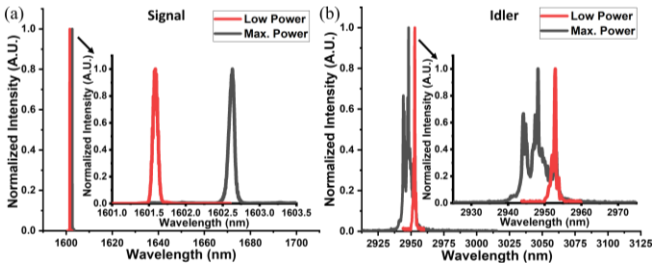

Fig. 7. Spectra of (a) signal and (b) idler for the HCF fiber-feedback OPO. The insets show the magnified spectra.

power with a slope efficiency of 48.7 % up to a maximum power of 3.10 W. The total power conversion efficiency at the maximum pump power was calculated to be 60.0 %.

The spectrum of the resonated signal from the OC was measured with a spectrum analyzer (OSA) (AQ6375, Yokogawa, 0.5-nm resolution) and is shown in Fig. 6(a). It can be clearly seen that the intra-cavity signal pulses underwent significant spectral broadening, probably due to SPM, through propagating in the SMF-28 fiber at high peak powers. The full width at half maximum (FWHM) of the signal spectrum ranged from 5.4 nm - 13.0 nm. The corresponding idler spectra at low and maximum output powers, measured with an OSA (721 series, Bristol instruments, 4-GHz resolution), is presented in Fig. 6(b). An increase in spectral width with pump power was observed from 10.5 nm - 29.0 nm FWHM. The central signal and idler wavelengths were 1594.6 nm and 2993.8 nm at low power and 1601.4 nm and 2996.6nm at maximum power, respectively. The very small discrepancy from the phase-matched wavelengths arises from the idler and signal spectra not being measured at the same time – any drift in the temperature of the crystal between measurements resulting in a shift in signal and idler wavelengths.

These significant nonlinear effects limit the power scalability of the fiber-feedback OPO system if one wishes to maintain the spectral width for applications. To reduce the nonlinearities within the OPO cavity, the solid-core SMF-28 feedback-fiber was replaced by a HCF feedback-fiber with atmospheric air as the guiding medium. With the HCF as the feedback-fiber, OPO operation was observed at a pump average-power threshold of 0.48 W. The output average power of the idler and signal with respect to different pump powers are presented in Fig. 5(b). The idler power increased linearly with respect to the pump power at a slope efficiency of 21.7 % up to a maximum generated power of 1.50 W, and the signal power also increased linearly with respect to the pump power with a slope efficiency of 44.8 % up to a maximum power of 3.02 W. The total power conversion efficiency at the maximum pump power was calculated to be 62.1 %. The maximum idler power for the fiber-feedback OPO setups described in this paper (1.24 W and 1.50 W) corresponds to pulse energies (peak powers) of 1.24 μJ (9.7 kW) and 1.50 μJ (11.7 kW) for the solid and hollow core fiber implementations respectively. To the best of our knowledge, these results represent the highest energy MIR pulses achieved from such OPOs.

The graphs in Fig. 7(a) show the signal spectra with 0.05-nm resolution for the HCF-fiber-feedback OPO, measured at the OC. The FWHM of the signal spectrum ranged from 0.07 – 0.09 nm. It can be seen that the signal spectrum is significantly narrower than that from the solid core SMF-28 fiber-feedback OPO (5.4 nm - 13.0 nm as described previously). Note that the slight wavelength shift at

maximum output power is due to the small temperature change of the PPLN crystal at higher pump powers. The idler spectra from the HCF fiber-feedback OPO, at low and maximum output powers, are presented in Fig. 7(b). The central signal and idler wavelengths were 1601.6 nm and 2952.9 nm at low power and 1602.6 nm and 2948.2 nm at maximum power, respectively. Compared with the solid-core SMF-28 fiber-feedback OPO, the idler spectral width from the HCF fiber-feedback OPO, as with the signal spectrum, is also much narrower, ranging from 0.48 - 8.38 nm. Note that the increase in spectral widths at high power (especially for the idler) can be accounted for by the increase in the pump's spectral width due to SPM in the fiber MOPA system, mainly from the final amplifier stage (Fig. 2(a)). The multipeak nature of the idler spectrum especially at high power arises from the multiple peaks of the pump spectrum, which again is due to SPM within the MOPA system. This SPM could be reduced through the use of active fibers with increased core size/dopant concentration. Nevertheless, the use of an HCF fiber as the OPO's feedback fiber has very successfully reduced the intracavity nonlinearities, leading to an improved power scalability of the OPO. Further power scaling work is currently underway.

The signal and idler wavelength tunability was also characterized using different PPLN grating periods and oven temperatures. Seamless wavelength tuning for the ranges 1472.0–1758.2 nm and 2559.1-3562.7 nm was achieved for the signal and idler outputs, respectively, as shown in Fig. 8. Note that OPO operation was only observed for four out of the five channels of the PPLN crystal. For the 31.59-µm-grating channel, the theoretical phase-matched signal wavelengths for crystal temperatures above 20 °C range from 1896 - 2040 nm. The loss of the HCF feedback-fiber is anticipated to be high across this waveband, if indeed it guides at all, moreover these wavelengths lie at the edge of the high reflectivity band of the curved cavity mirrors. As a consequence, it was not possible to achieve OPO laser oscillation with this channel.

The output signal pulses of the OPOs were also measured. The spectral broadening arising from the high intracavity nonlinearities of the solid-core fiber-feedback OPO also caused an increase in pulse width due to the high dispersion of the solid-core feedback-fiber, resulting in an increase in pulse width from 120 ps to 170ps. By contrast, the HCF fiber-feedback OPO generated signal pulses with a constant width of around 120 ps due to the negligible nonlinearity and smaller dispersion. Note that the output idler pulses were not measured due to a lack of suitable instrument, however we would expected those to have a similar width to that of the pump, which also explains the higher power conversion from the HCF fiber-feedback OPO due to the better temporal overlap between the interacting pulses.

In conclusion, we present a high-pulse-energy, MIR, picosecond fiber-feedback OPO at a 1-MHz repetition rate. Tunable signal and idler wavelength ranges of 1472.0–1758.2 nm and 2559.1-3562.7 nm, respectively, were realized. Using a solid-core SMF-28 fiber as the feedback fiber, significant spectral broadening was observed due to the strong nonlinear effects arising from high nonlinearity of the long fiber length. This would limit the power scalability of the system at a high-brightness level. The intracavity nonlinearity was significantly reduced through the use of a HCF fiber as the feedback fiber. The OPO generates MIR pulses with a pulse energy of up to 1.50 µJ (11.7 kW peak power). To the best of our knowledge, these results represent the highest energy MIR pulses achieved from fiber-feedback OPOs and represents the first use of an HCF in such a system.

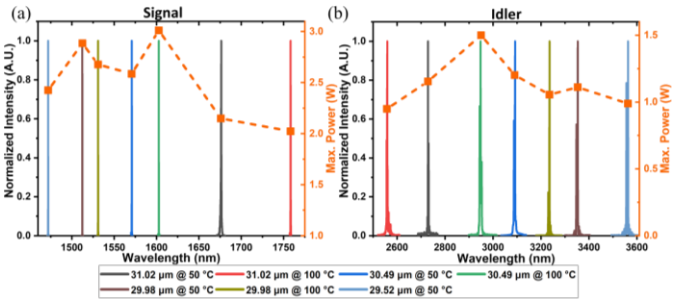

Fig. 8. Tunability of the (a) signal and (b) idler from the fiber-feedback OPO and the corresponding maximum power.

Funding. Engineering and Physical Sciences Research Council (EPSRC) (AirGuide Photonics Programme Grant (EP/P030181/1), Laser Technologies for Future Manufacturing Platform Grant (EP/P027644/1), InLightenUs Transformative Healthcare 2050 project (EP/T020997/1)), European Research Council (ERC) (Lightpipe, grant agreement no.682724).

Acknowledgment. The authors would like to thank Emeritus professor David Shepherd from the Optoelectronics Research Centre for the useful discussions. For the purpose of open access, the author has applied a creative commons attribution (CC BY) licence (where permitted by UKRI, 'open government licence' or 'creative commons attribution no-derivatives (CC BY-ND) licence' may be stated instead) to any author accepted manuscript version arising.

Disclosures. The authors declare no conflict of interest.

Data availability. Data underlying the results presented in this paper are available at https://doi.org/10.5258/SOTON/D2274.

REFERENCES

1. M. W. Sigrist, Journal of Advanced Research **6,** 529 (2015).
2. R. Knappe, H. Haloui, A. Seifert, A. Weis, and A. Nebel, Laser-based Micro- and Nano-packaging and Assembly IV **7585,** 150 (2010).
3. Y. Su, W. Wang, X. Hu, H. Hu, X. Huang, Y. Wang, J. Si, X. Xie, B. Han, H. Feng, Q. Hao, G. Zhu, T. Duan, and W. Zhao, Opt. Express **26,** 34515 (2018).
4. A. Urich, R. R. J. Maier, Fei Yu, J. C. Knight, D. P. Hand, and J. D. Shephard, Biomed. Opt. Express **4**, 193 (2013)
5. Q. Fu, L. Xu, S. Liang, P. C. Shardlow, D. P. Shepherd, S. Alam, and D. J. Richardson, Opt. Express **28,** 5741 (2020).
6. Charles W. Rudy, Alireza Marandi, Kirk A. Ingold, Stephen J. Wolf, Konstantin L. Vodopyanov, Robert L. Byer, Lihmei Yang, Peng Wan, and Jian Liu, Opt. Express **20,** 27589 (2012).
7. L. Xu, H.-Y. Chan, S.-U. Alam, D. J. Richardson, and D. P. Shepherd, Opt. Lett. **40,** 3288 (2015).
8. K. Wei, P. Jiang, B. Wu, T. Chen, and Y. Shen, Chinese Physics B **24,** 024217 (2015).
9. T. Südmeyer, E. Innerhofer, F. Brunner, R. Paschotta, T. Usami, H. Ito, S. Kurimura, K. Kitamura, D. C. Hanna, and U. Keller, Opt. Lett. **29,** 1111 (2004)
10. Tobias Steinle, Florian Mörz, Andy Steinmann, and Harald Giessen, Opt. Lett. **41,** 4863 (2016)
11. K. A. Ingold, A. Marandi, M. J. F. Digonnet, and R. L. Byer, Opt. Lett. **40,** 4368 (2015).
12. Callum F. O'Donnell, S. Chaitanya Kumar, T. Paoletta, and M. Ebrahim-Zadeh, Optica **7,** 426 (2020).
13. Florian Kienle, Peh Siong Teh, Shaif-Ul Alam, Corin B. E. Gawith, David C. Hanna, David J. Richardson, and David P. Shepherd, Opt. Lett. **35,** 3580 (2010).

14. F. Poletti, Opt. Express **22**, 23807 (2014).
15. G. A. Sanders, A. A. Taranta, C. Narayanan, E. N. Fokoua, S. A. Mousavi, L. K. Strandjord, M. Smiciklas, T. D. Bradley, J. Hayes, G. T. Jasion, and T. Qiu, Opt. Lett. **46**, 46 (2021).